Skyrmions induced by dissipationless drag in U(1)×U(1) superconductors

Julien Garaud,[1,2] Karl A. H. Sellin,[2] Juha Jäykkä,[3] and Egor Babaev[1,2]
[1]*Department of Physics, University of Massachusetts Amherst, Massachusetts 01003, USA*
[2]*Department of Theoretical Physics, Royal Institute of Technology, Stockholm, SE-10691 Sweden*
[3]*Nordita, KTH Royal Institute of Technology and Stockholm University, Stockholm, SE-10691 Sweden*
(Received 12 July 2013; revised manuscript received 15 February 2014; published 7 March 2014)

Rather generically, multicomponent superconductors and superfluids have intercomponent current-current interaction. We show that in superconductors with substantially strong intercomponent drag interaction, the topological defects which form in an external field are characterized by a skyrmionic topological charge. We then demonstrate that they can be distinguished from ordinary vortex matter by a very characteristic magnetization process due to the dipolar nature of inter-skyrmion forces. The results provide an experimental signature to confirm or rule out the formation p-wave state with reduced spin stiffness in p-wave superconductors.

DOI: 10.1103/PhysRevB.89.104508 PACS number(s): 74.25.Ha, 12.39.Dc, 74.25.Uv

In multicomponent superconductors and superfluids, the intercomponent current-current interaction is rather generic. It usually assumes the form of the scalar product of supercurrents in the two components $\mathcal{F}_d \propto \boldsymbol{J}_1 \cdot \boldsymbol{J}_2$. This kind of interaction between components can have various microscopic origins. It was discussed in connection with ^{3}He-^{4}He mixtures [1], components of order parameters of spin-triplet superfluids and superconductors [2–5], hadronic superfluids in neutron stars [6–10], metallic hydrogen and deuterium [11,12], ultracold atomic mixtures [13,14], and strongly correlated atomic mixtures in optical lattices [15]. In the latter case, it was shown that it could be tuned to have arbitrary strength (in relative units) [15]. This kind of interaction for example affects rotational response of neutron stars [8] and phase transitions, phase diagrams, and rotational response of superfluid mixtures [12,16–21]. Despite the generic character of such interaction, much less is known about its effect on the properties of topological excitations and magnetic response, beyond the simplest London approximation. In particular, little is known about collective properties of such defects. Here, we address this problem. We show that beyond a certain interaction threshold, the topological defects in the system acquire a skyrmionic topological charge. This results in long-range inter-skyrmion forces which alter dramatically the collective behavior of vortex matter.

Note that current-current interaction is fourth order in the order parameters densities and second order in their derivatives. Importantly, it is not positively defined. Because the total free energy is positively defined, the drag term should come with other high-power terms consistent with the U(1) × U(1) symmetry. Details of the model and how it relates to usual London models are discussed in Appendix A. The precise form of these terms is not principally important for the purpose of this work, so we investigate a minimal Ginzburg-Landau (GL) model, which is positively defined and has the correct London limit [1]

$$\mathcal{F} = \frac{\boldsymbol{B}^2}{2} + \sum_{a=1,2} \frac{1}{2}|\boldsymbol{D}\psi_a|^2 + \alpha_a|\psi_a|^2 + \frac{1}{2}\beta_a|\psi_a|^4 \quad (1a)$$

$$+ \frac{\nu}{2}|\mathrm{Im}(\psi_1^* \boldsymbol{D}\psi_1) + \mathrm{Im}(\psi_2^* \boldsymbol{D}\psi_2)|^2. \quad (1b)$$

Here, $\psi_a = |\psi_a| e^{i\varphi_a}$ are complex fields representing the independently conserved superconducting condensates denoted by indices $a = 1,2$. The term (1b) contains the intercomponent current interaction as well as higher-order terms which makes the free energy bounded from below. Aside from the drag interaction, the condensates are coupled by electromagnetic interactions in the kinetic terms $\boldsymbol{D} = \boldsymbol{\nabla} + ie\boldsymbol{A}$. We set the Cooper-pair charge as twice the electronic charge, then in these units the coupling constant e parametrizes the London penetration length of the magnetic field $\boldsymbol{B} = \boldsymbol{\nabla} \times \boldsymbol{A}$, and the supercurrent reads as $\boldsymbol{J} \equiv \Sigma_a \boldsymbol{J}_a = [1 + \nu\Sigma_b|\psi_b|^2]\Sigma_a \mathrm{Im}(\psi_a^* \boldsymbol{D}\psi_a)$. In connection with spin-triplet systems, such models are discussed in the situations where the variations of the relative phase $\varphi_2 - \varphi_1$ of the condensates variations are associated with spin degrees of freedom. The drag interaction is then associated with the spin stiffness [2,3].

In this work, we consider a two-dimensional model. The discussions thus also apply to three-dimensional systems invariant along the direction normal to the plane. The elementary topological excitations of the model are fractional vortices. These are field configurations with a 2π phase winding only in one phase (e.g., φ_1 has $\oint \boldsymbol{\nabla}\varphi_1 = 2\pi$ winding while $\oint \boldsymbol{\nabla}\varphi_2 = 0$). A fractional vortex in the a condensate carries a fraction of flux quantum $\Phi_a = \oint \boldsymbol{A}\, d\boldsymbol{\ell} = \frac{|\psi_a|^2}{\varrho^2}\frac{1}{e}\oint \boldsymbol{\nabla}\varphi_a = \frac{|\psi_a|^2}{\varrho^2}\Phi_0$ with the flux quantum $\Phi_0 = 2\pi/e$ and the total superfluid density $\varrho^2 = \Sigma_a|\psi_a|^2$. Note that this flux quantization is the same as in two-component superconductors without drag [22]. Fractional vortices have logarithmically divergent energy. However, a composite vortex being the bound state of fractional vortices in both condensates (each phase φ_a winds 2π) has finite energy and carries an integer flux [22] (see details of the derivation in Appendix A). In the London limit of a U(1) × U(1) superconductor, fractional vortices can be described by point-like particles interacting through logarithmic two-dimensional Coulomb and Yukawa interactions, which read in the general case (see details of the derivation in Appendix A) as

$$E_{11} = \ln\frac{R}{x} + wmK_0\left(\frac{x}{\lambda}\right), \quad E_{22} = \ln\frac{R}{x} + \frac{w}{m}K_0\left(\frac{x}{\lambda}\right),$$

$$E_{12} = -\ln\frac{R}{x} + wK_0\left(\frac{x}{\lambda}\right). \quad (2)$$

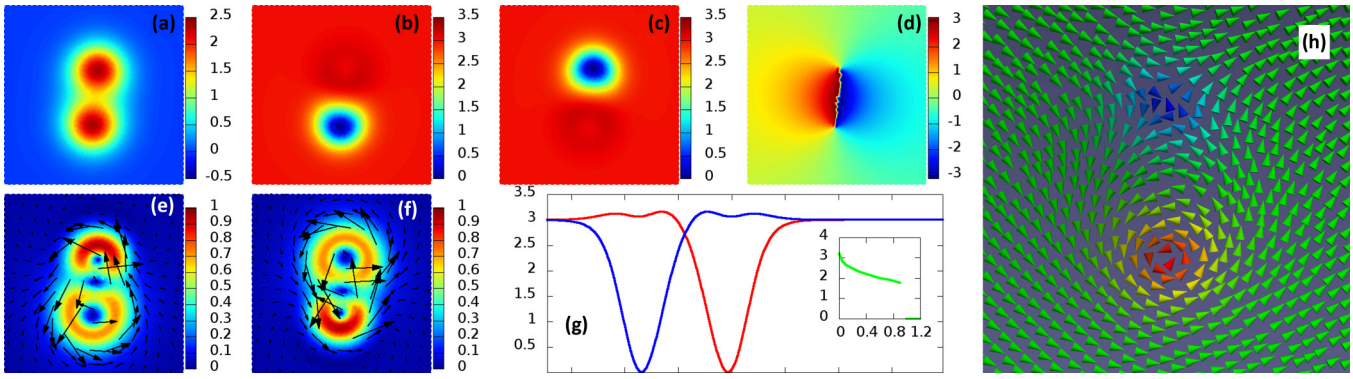

FIG. 1. (Color online) A bound state of fractional vortices with $e = 0.2$ and the potential parameters $(\alpha_a, \beta_a) = (-3.0, 1.0)$. The drag coupling is $\nu = 2.0$. Displayed quantities are the magnetic flux (a) and the densities of superconducting condensate $|\psi_1|^2$ (b) and $|\psi_2|^2$ (c). (d) Shows the phase difference $\varphi_2 - \varphi_1$, while individual currents $|\boldsymbol{J}_1|$ and $|\boldsymbol{J}_2|$ are respectively displayed in (e) and (f). Both currents circulate around each core due to drag effect. (g) Shows cross section of densities $|\psi_1|^2$ (red) $|\psi_2|^2$ (blue) along the y axis. Note the deformed w-shaped modulation of densities above singularities of the other condensate. The inset shows the distance between cores as a function of the Josephson coupling. At such sufficiently strong coupling, skyrmions collapse. The rightmost panel (h) displays the normalized projection of the psuedospin $\mathbf{n}$ onto the plane, while colors give the magnitude of n_z. Blue corresponds to the south pole (-1) while red is the north pole $(+1)$ of the target sphere S^2.

Here, the interacting energies $E_{\rm ab}$, between vortices in the a and b condensates, are expressed in units of $2\pi|\psi_1|^2|\psi_2|^2/\varrho^2$. K_0 is the modified Bessel of the second kind and R denotes the system size while the parameters m and w are $m = \frac{|\psi_1|^2}{|\psi_2|^2}$ and $w = 1 + \nu\varrho^2$. $\lambda = \frac{1}{e\sqrt{w\varrho^2}}$ is the penetration length of the magnetic field. For vanishing drag ($w = 1$), the minimum energy corresponds to an axially symmetric state of two cocentered fractional vortices [22]. There, the Coulomb and Yukawa contributions in E_{12} interaction compensate at $x = 0$ [23]. The drag term (1b) (i.e., when $w > 1$) penalizes codirected currents so the Coulomb and Yukawa contributions of the interacting energy E_{12} no longer cancel at $x = 0$ but at some finite separation. In the case of half-quantum vortices, this process was studied in detail in the London model [4].

Here, we investigate the structure of single-vortex and multivortex states, beyond the London limit. To this end, we numerically minimize the free energy (1) within a finite-element framework provided by the FREEFEM++ library [24] (see technical details in Appendix C). We find that in contrast to the London limit, weak drag does not produce numerically detectable splitting of vortex cores. This is connected with the existence of finite cores where the current is modulated by a density suppression. Larger drag splits a composite vortex into a bound state of well-separated fractional vortices. This is shown on Fig. 1. Note that a single fractional vortex has nontrivial structure. In particular, its magnetic field is not exponentially localized and can exhibit flux inversion [25]. Figure 1 shows that some of the features of isolated fractional vortices, reported in [25] such as w-shaped modulation of densities, are preserved in the split composite vortex.

In general, in multicomponent superconductors there could be terms which break the U(1) × U(1) symmetry explicitly. A typical example is $-\eta|\psi_1||\psi_2|\cos\varphi_{12}$. Such terms result in asymptotically linear confinement of fractional vortices. We find that when such terms are not very strong, the splitting of cores is still present as shown on Fig. 1(g). In such a case, dipolar forces are still present, but suppressed at the Josephson length.

The bound state of well-separated fractional vortices is a *skyrmion*. This follows from mapping the two-component model (1) to an easy-plane nonlinear σ model [11,26]. There, the pseudospin unit vector $\mathbf{n}$ is the projection of superconducting condensates on spin-$\frac{1}{2}$ Pauli matrices $\boldsymbol{\sigma}$: $\mathbf{n} = \frac{\Psi^\dagger\boldsymbol{\sigma}\Psi}{\Psi^\dagger\Psi}$ where $\Psi^\dagger = (\psi_1^*, \psi_2^*)$. When there is nonzero drag, the free energy (1) can be written in $\mathbf{n}$ representation as

$$\mathcal{F} = \frac{1}{2}(\boldsymbol{\nabla}\varrho)^2 + \frac{\varrho^2}{8}\partial_i n_a \partial_i n_a + \frac{\boldsymbol{J}^2}{2e^2 w\varrho^2} + V(\varrho, n_z) + \frac{1}{2e^2}\left\{\varepsilon_{ijk}\left[\partial_i\left(\frac{J_j}{ew\varrho^2}\right) - \frac{1}{4}\varepsilon_{abc} n_a \partial_i n_b \partial_j n_c\right]\right\}^2, \quad (3)$$

where ε is the Levi-Civita symbol and V stands for the potential terms in (1a) (see Appendix A for details of this derivation). The pseudospin is a map $\mathbf{n} : S^2 \to S^2$, classified by the homotopy class $\pi_2(S^2) \in \mathbb{Z}$, thus defining the integer-valued topological (skyrmionic) charge $\mathcal{Q}(\mathbf{n}) = \frac{1}{4\pi}\int_{\mathbb{R}^2} \mathbf{n}\cdot\partial_x\mathbf{n}\times\partial_y\mathbf{n}\, dx\, dy$. Ordinary (composite) vortices with a single core $\Psi = 0$ have $\mathcal{Q} = 0$. Here, the core-split vortices have nontrivial skyrmionic charge $\mathcal{Q} = N$, the number of flux quanta. The quantization of $\mathcal{Q}$ is related to the flux quantization, and $\Phi = \mathcal{Q}\Phi_0$ as long as cores are split ($\Psi \neq 0$).

The calculated pseudospin texture of $\mathbf{n}$ is shown on Fig. 1(h). Numerically calculated topological charge was found to be an integer (with a negligible error of order 10^{-4}).[1] Note that these skyrmions are quite different from the skyrmions or nonaxially symmetric vortices considered in superconducting states with different number of components and symmetries [27–35]. In particular, the structural differences in these skyrmions dictate different inter-skyrmion forces. This

[1]Note that the topological charge is an integer only for when a skyrmion is sufficiently far from boundaries. Since when simulating a finite sample in applied field, there are states where only part of the skyrmion texture enters the sample, in general the topological charge $\mathcal{Q}$ will not be integer.

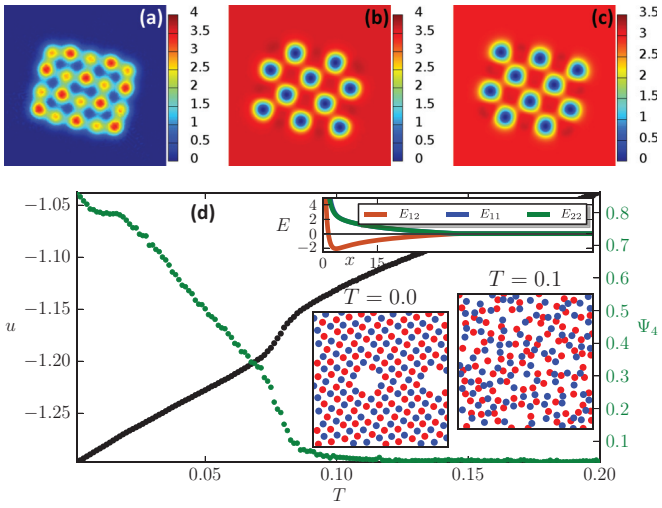

FIG. 2. (Color online) A $\mathcal{Q} = 10$ quanta configuration bound by dipolar forces. Parameters are $(\alpha_1,\beta_1) = (-3.6,1.0)$, $(\alpha_2,\beta_2) = (-3.0,1.0)$ with $e = 0.6$ and the drag coupling $\nu = 2.0$. Displayed quantities are the magnetic flux (a) and the densities of superconducting condensate $|\psi_1|^2$ (b) and $|\psi_2|^2$ (c). Lower panel (d) shows a Monte Carlo simulation of hundred point particles of each kind interacting according to (2), with 0.036 particles per surface area which allows us to emulate the skyrmionic lattice melting process. Here, u is the total interaction energy per particle and Ψ_4 is the square lattice order parameter (see Appendix C). They show a melting transition to a state which has no square lattice ordering but still has bound pairs. Insets show low- and high-temperature states, as well as the interaction energies.

warrants investigation of a state of such a superconductor in external field, which we address in the following.

The mapping of fractional vortices to Coulomb charges (2) suggests that there will be asymptotically power-law inter-skyrmion dipolar interaction forces (attractive for certain orientations and repulsive for other). Indeed, the long-range Coulomb interaction originates in the phase difference mode $\varphi_{12} \equiv \varphi_2 - \varphi_1$ [23]. For the pair of fractional vortices, it has a clear dipolelike structure shown on Fig. 1(d). The total interaction forces, beyond the London limit, do not reduce to Coulomb and Yukawa forces and are especially complicated at shorter distances due to the presence of density modes and Skyrme-like terms in (3). To investigate multiquanta states, we compute configurations carrying several flux quanta by energy minimization. First, as displayed in the first line in Fig. 2, they can form compact "checkerboard" cluster. Unlike type-1.5 vortex clusters, where (composite) vortices can form cluster with inner triangular ordering [36–38], the dipolar-attraction-driven structures have compact lattices with two interlaced square lattices.[2] Other kinds of structures which we found for few vortex states are looplike and stripelike structures. These are shown on Fig. 3 and details about these configurations are included Appendix B. Some of these configurations are metastable local minima. The trend which we observed is that with increasing the drag coupling, multiple quanta configurations become more compact. Remarkably, some of the vortex structures which we obtain are quite similar to those appearing in the easy-plane baby-Skyrme model consisting of the pseudospin $\mathbf{n}$ alone [40]. This similarity in structures is an interesting fact which could not be *a priori* expected because $\mathbf{n}$ represents only a part of the degrees of freedom of GL theory (3), and does not account for all intervortex interaction forces. Moreover, at short length scales, the GL model is certainly principally different from the Skyrme model [11]. Our observations demonstrate that at least in two dimensions there is a very close relationship between structure formation of topological defects in multicomponent superconductors and in pure baby-Skyrme models. Aside from that, we find that structure formation exhibits also complicated octagonal looplike periodic structure as in the first line in Fig. 4. Their elementary cell carries $\mathcal{Q} = 4$ flux quanta, and assumes octagonal geometry as a result of rotated underlying square fractional vortex structures.

Since the dipolar interactions are long range, they should dominate the tail of inter-skyrmion interactions. We therefore examine how much of the structure formation can be reproduced in the toy model of interacting point charges (2). To this end, we perform Monte Carlo (MC) simulations using the Metropolis algorithm with parallel tempering [41]. Although the point-charge model does not perfectly capture all the underlying physics, it reproduces some aspects of the structures obtained beyond the London limit (see Figs. 2 and 4). Moreover, the MC approach allows us to investigate how the ordering depends on temperature. As shown on Figs. 2(d) and 4(d), thermal fluctuations can cause unbinding of the crystalline multiquanta skyrmionic bound states held by dipolar forces. However, fractional vortices are still paired and constitute well-defined skyrmions in higher-temperature phases where there is no lattice structure.

Finally, we address the magnetization process of the skyrmionic state. To this end, we simulate the Gibbs free energy $\mathcal{G} = \mathcal{F} - \boldsymbol{B} \cdot \mathbf{H}$ of the system (1), on a finite domain in an increasing external field $\boldsymbol{H} = H\boldsymbol{e}_z$. Here, finite differences are used instead of finite elements, and a quasi-Newton Broyden-Fletcher-Goldfarb-Shanno (BFGS) method instead of conjugate gradients. For details, see [42] and Appendix C. The magnetization process of the skyrmionic states is quite specific. It can be easily distinguished from other unconventional magnetization processes such as those of chiral p-wave superconductors with multidomains [43], entropically stabilized square lattices [44], and type-1.5 superconductors [36,38]. As shown on Fig. 5, it is heavily influenced by the existence of dipolar forces. In these simulations, we typically observed that multi-skyrmion domains bound by dipolar forces are formed near boundaries. These domains are attracted to boundaries by long-range dipolar interaction with image charges. This crucially modifies Bean-Livingston barrier physics because dipolar attraction to the image "anti-skyrmions" has longer range than the repulsion from the boundary due to surface Meissner current. These domains gradually fill the system until merging to form a (checkerboard) square lattice of fractional vortices. When the field is increased

[2]Note that formation of checkerboard square lattices for p-wave superconductors near H_{c2} was found in [5,39]. Here, we consider a different situation of vortex cluster formed due to attractive dipolar interactions.

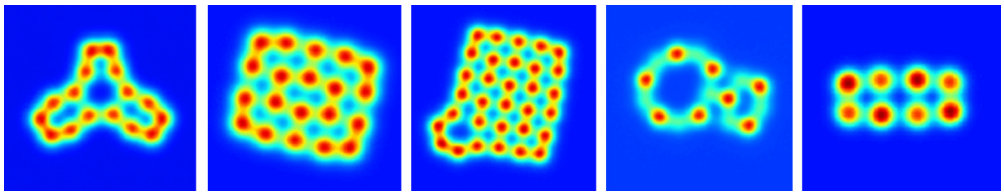

FIG. 3. (Color online) Profile of the magnetic field for various bound states of vortices in the model (1), carrying $N = 8$, 10, 16, 8, and 4 flux quanta, respectively. The corresponding potential parameters and details of the other physical quantities are given in Appendix B. Note that some regimes have extra biquadratic density potential term ($\sim|\psi_1|^2|\psi_2|^2$) which is not essential but enriches the observed structures.

further, the density of skyrmions in the square lattice grows. Importantly, during the magnetization process, the skyrmionic charge does not change in integer steps. When the condensates are not equivalent, there is a layer of one kind of fractional vortices (or half-skyrmions) near boundaries as can be seen in Fig. 5. This is in agreement with the thermodynamical stability of fractional vortices near boundaries demonstrated by Silaev in the London limit without drag [45].

In conclusion, we investigated topological defects and magnetic response of U(1) × U(1) superconductors with dissipationless drag, beyond the commonly used London approximation. In contrast to the London limit, it requires a critical strength of dissipationless drag to form unconventional split vortex solutions. We demonstrated that split fractional vortices in this model have a well-defined skyrmionic charge. We established that, when the model is U(1) × U(1) or softly broken U(1) × U(1), the vortex lattice structure is dominated by the long-range dipolar inter-skyrmion forces. This results in unconventional magnetic response in low fields which features lack of hexagonal vortex lattice and formation of a layer of square lattice growing inward from boundaries of the sample.

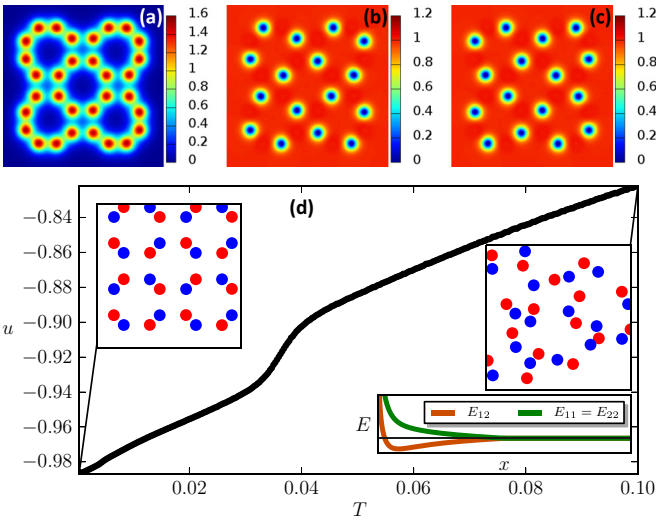

FIG. 4. (Color online) A structure carrying $\mathcal{Q} = 16$ flux quanta. The elementary cell here is a $\mathcal{Q} = 4$ skyrmion. The parameters are $(\alpha_a, \beta_a) = (-5.0, 5.0)$ with $e = 0.6$ and the drag coupling $\nu = 2.0$. Displayed quantities are the same as in Fig. 2. Lower panel shows (d) shows a Monte Carlo simulation of 16 particles of each kind for 0.036 particles per surface area. In the low-temperature phase, the fractional vortices are paired and ordered in a lattice, and for higher temperature the lattice melts but the vortices are still paired.

This magnetization process can be easily identified for example in scanning SQUID measurements and discriminated from other models for p-wave superconductivity which by contrast predict hexagonal vortex lattices in low fields and square lattice in high fields. It can also be straightforwardly distinguished from that of ordinary single-component type-II superconductors or multicomponent type-1.5 superconductors or chiral p-wave multidomain superconductors. For example, the magnetic behavior of the putative triplet superconductor Sr_2RuO_4 is nontrivial, featuring phase separation [47–51]. However, since square vortex lattices were observed only at elevated fields and no boundary vortex states were reported, it is inconsistent with models which have long-range skyrmionic forces.

We thank J. Carlström for discussions. This work is supported by the Swedish Research Council by the Knut and Alice Wallenberg Foundation through the Royal Swedish Academy of Sciences fellowship and by NSF CAREER Award No. DMR-0955902. The computations were performed on resources provided by the Swedish National Infrastructure for Computing (SNIC) at National Supercomputer Center at Linkoping, Sweden.

APPENDIX A: DETAILS OF THEORETICAL FRAMEWORK

In two-component superconductors, the elementary topological excitations are fractional vortices. These are field configurations having a 2π phase winding only in one phase (e.g., φ_1 has $\oint \nabla\varphi_1 = 2\pi$ winding while $\oint \nabla\varphi_2 = 0$). The physics of fractional vortices, as well as the role of the intercomponent dissipationless drag, can be enlightened by rewriting the theory in terms of *charged* and *neutral* modes. Here, we derive the interaction between fractional vortices for a two-component system. In particular, this shows how, in the London limit, fractional vortices can be treated as point particles with Coulomb and Yukawa interactions. The Ginzburg-Landau free energy functional reads as

$$\mathcal{F} = \frac{1}{2}(\nabla \times \boldsymbol{A})^2 + \sum_a \frac{1}{2}|\boldsymbol{D}\psi_a|^2 \tag{A1a}$$

$$+ \sum_a \alpha_a|\psi_a|^2 + \frac{1}{2}\beta_a|\psi_a|^4 \tag{A1b}$$

$$+ \frac{1}{2}\gamma|\psi_1|^2|\psi_2|^2 \tag{A1c}$$

$$+ \frac{\nu}{2}\left|\mathrm{Im}(\psi_1^*\boldsymbol{D}\psi_1) + \mathrm{Im}(\psi_2^*\boldsymbol{D}\psi_2)\right|^2 . \tag{A1d}$$

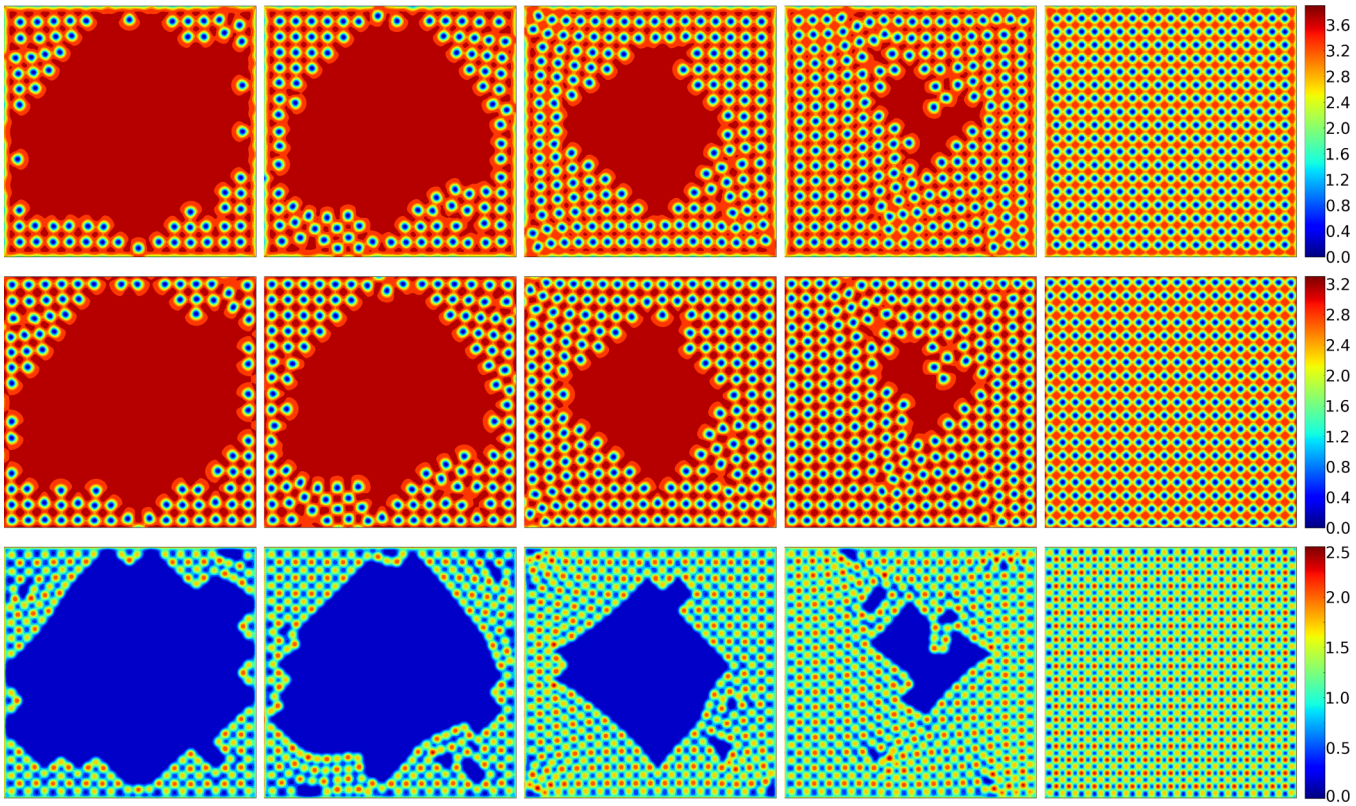

FIG. 5. (Color online) Sequences of the skyrmionic states in in the magnetization process of a finite sample in slowly increased magnetic flux. Corresponding values of the applied flux are respectively 96, 129, 201, 258, and 381 (in the unit of the flux quantum). Parameters of the Ginzburg-Landau free energy are the same as in Fig. 2. First line shows $|\psi_1|^2$, second line $|\psi_2|^2$, while the third displays the magnetic field $\boldsymbol{B}$. The peaks of different intensities in the magnetic field correspond to vortices carrying different fractions of flux quantum. Note that there is a layer of half-skyrmions near the boundary. This is consistent with the thermodynamic stability of fractional vortices near boundaries as discussed in [45]. Animations of the magnetization process are available as online Supplemental Material [46].

Note that, for completeness, we added biquadratic density coupling (A1c) to the potential energy. Obviously, its effect is to enforce core splitting of fractional (when $\gamma > 0$) vortices. Since we mostly focus on the role of the drag interaction, the biquadratic density term is introduced here for sake of completeness rather than an essential ingredient of the physics we discuss.

1. Parametrization of the intercomponent drag and its London limit

Traditionally, the intercomponent current-current interaction is parametrized as the scalar product of supercurrents of two components $\mathcal{F}_d \propto \boldsymbol{J}_1 \cdot \boldsymbol{J}_2$. Beyond the London limit, such a term reads explicitly as $\mathcal{F}_d \propto \mathrm{Im}(\psi_1^* \boldsymbol{D}\psi_1) \cdot \mathrm{Im}(\psi_2^* \boldsymbol{D}\psi_2)$. This term is fourth order in the order-parameter densities and second order in their derivatives, moreover, it is not positively defined. This leads to an unphysical instability: by creating strong counterdirected currents and increasing density, in a minimal GL model with such a term, makes free energy negative and unbounded from below. Thus, this term should come with other high-power terms consistent with the symmetry, which make the total free energy positively defined. The precise form of these terms is not principally important for the purpose of this work, so we choose to use (A1d), which is obviously positive. However, one should also make sure that this term has the proper London limit. There, the free-energy functional (A1a)–(A1d) reads as

$$\mathcal{F} = \frac{1}{2}(\boldsymbol{\nabla} \times \boldsymbol{A})^2 + \sum_a \frac{1}{2}|\boldsymbol{D}\psi_a|^2 \tag{A2a}$$

$$+ \frac{\nu}{2}|\mathrm{Im}(\psi_1^* \boldsymbol{D}\psi_1) + \mathrm{Im}(\psi_2^* \boldsymbol{D}\psi_2)|^2. \tag{A2b}$$

Since the densities are constant, the covariant derivative reads as $\boldsymbol{D}\psi_a = i|\psi_a|(\boldsymbol{\nabla}\varphi_a + e\boldsymbol{A})e^{i\varphi_a}$ and thus, expanding the drag term (A2b) and collecting various orders, the free energy assumes the form typically used for discussing the problem in the London limit

$$\mathcal{F} = \frac{1}{2}(\boldsymbol{\nabla} \times \boldsymbol{A})^2 + \sum_{a=1,2} \frac{1}{2}\rho_{aa}(\boldsymbol{\nabla}\varphi_a + e\boldsymbol{A})^2 \tag{A3a}$$

$$+ \rho_d(\boldsymbol{\nabla}\varphi_1 + e\boldsymbol{A}) \cdot (\boldsymbol{\nabla}\varphi_2 + e\boldsymbol{A}), \tag{A3b}$$

where the prefactors are

$$\rho_{aa} = |\psi_a|^2(1 + \nu|\psi_a|^2), \quad \rho_d = \nu|\psi_1|^2|\psi_2|^2. \tag{A4}$$

The term (A3b) is the scalar product of the supercurrents of two components. Thus, our parametrization (A1d) of intercomponent current-current interaction has the conventional London limit.

2. Derivation of neutral and charged modes

To understand the role of the fundamental excitations (i.e., fractional vortices), the Ginzburg-Landau free energy (A1a)–(A1d) can be rewritten into *charged* and *neutral* modes by expanding the kinetic term (A1a) and the drag term (A1d)

$$\mathcal{F} = \frac{1}{2}(\nabla \times \boldsymbol{A})^2 + \frac{\boldsymbol{J}^2}{2e^2 w\varrho^2} \tag{A5a}$$

$$+ \sum_a \frac{1}{2}(\nabla|\psi_a|)^2 + \alpha_a|\psi_a|^2 + \frac{\beta_a}{2}|\psi_a|^4 \tag{A5b}$$

$$+ \gamma|\psi_1|^2|\psi_2|^2 \tag{A5c}$$

$$+ \frac{|\psi_1|^2|\psi_2|^2}{2\varrho^2}(\nabla\varphi_{12})^2. \tag{A5d}$$

Here, $\varphi_{12} \equiv \varphi_2 - \varphi_1$ is the phase difference and

$$w = 1 + \nu\varrho^2 \quad \text{and} \quad \varrho^2 = \sum_a |\psi_a|^2. \tag{A6}$$

The supercurrent defined from the Ampère's equation $\nabla \times \boldsymbol{B} + \boldsymbol{J} = 0$ reads as

$$\boldsymbol{J}/e = ew\varrho^2\boldsymbol{A} + \sum_a |\psi_a|^2\nabla\varphi_a + \nu(|\psi_1|^2 + |\psi_2|^2)(|\psi_1|^2\nabla\varphi_1 + |\psi_2|^2\nabla\varphi_2) \tag{A7a}$$

$$= ew\varrho^2\boldsymbol{A} + w\sum_a |\psi_a|^2\nabla\varphi_a, \tag{A7b}$$

while the supercurrent associated with a given condensate reads as

$$\boldsymbol{J}_a = e\,\mathrm{Im}(\psi_a^*\boldsymbol{D}\psi_a)(1 + \nu|\psi_a|^2) + |\psi_a|^2\nu e\,\mathrm{Im}(\psi_b^*\boldsymbol{D}\psi_b), \tag{A8}$$

with the band index $b \neq a$. The term on the second line is the current of the component a induced (dragged) by the component b. Assuming phase winding in all components and since far away from a vortex $\boldsymbol{J}$ decays exponentially, the magnetic flux reads as

$$\Phi = \int \boldsymbol{B}\,dS = \oint \boldsymbol{A}\,d\ell = \frac{1}{e^2 w\varrho^2}\oint\left(\boldsymbol{J} - ew\sum_a |\psi_a|^2\nabla\varphi_a\right)d\ell = \Phi_0\sum_a \frac{|\psi_a|^2}{\varrho^2}, \tag{A9}$$

where $\Phi_0 = 2\pi/e$ is the flux quantum and the closed path integration is done so that the flux is positive. The flux $|\psi_a|^2\Phi_0/\varrho^2$ carried by a fractional vortex is the same as that of two-component superconductors without drag [22]. The London limit assumes that $|\psi_a| = \text{const}$ everywhere in space except small vortex core sharp cutoff. The expression (A5a)–(A5d) thus further simplifies

$$\mathcal{F} = \frac{1}{2}\left(\boldsymbol{B}^2 + \frac{1}{e^2 w\varrho^2}|\nabla \times \boldsymbol{B}|^2\right) \tag{A10a}$$

$$+ \frac{|\psi_1|^2|\psi_2|^2}{2\varrho^2}(\nabla\varphi_{12})^2, \tag{A10b}$$

where the Ampère's law has been used to replace the current in (A10a). The interaction energy of two nonoverlapping fractional vortices can be approximated in this London limit by considering *charged* (A10a) and *neutral* modes (A10b), separately. With the identity

$$|\nabla \times \boldsymbol{B}|^2 = \boldsymbol{B}\cdot\nabla\times\nabla\times\boldsymbol{B} - \nabla\cdot(\boldsymbol{B}\times\nabla\times\boldsymbol{B}), \tag{A11}$$

the energy of the *charged* sector (A10a) finally reads as

$$F_{\text{Charged}} = \int \frac{\boldsymbol{B}}{2}\left(\boldsymbol{B} + \frac{1}{e^2 w\varrho^2}\nabla\times\nabla\times\boldsymbol{B}\right). \tag{A12}$$

The London equation for a (pointlike) vortex placed at $\boldsymbol{x}_a$ and carrying a flux Φ_a is

$$\frac{1}{e^2 w\varrho^2}\nabla\times\nabla\times\boldsymbol{B} + \boldsymbol{B} = \Phi_a\delta(\boldsymbol{x} - \boldsymbol{x}_a), \tag{A13}$$

and its solution is

$$\boldsymbol{B}_a(\boldsymbol{x}) = \frac{\Phi_a e^2 w\varrho^2}{2\pi}K_0\left(\frac{|\boldsymbol{x} - \boldsymbol{x}_a|}{\lambda}\right). \tag{A14}$$

Here, the London penetration length is $\lambda = \frac{1}{e\sqrt{w\varrho^2}}$ and K_0 is the modified Bessel of second kind. For two vortices located at $\boldsymbol{x}_a$ and $\boldsymbol{x}_b$, and carrying fluxes Φ_a and Φ_b, the source term in London equation reads as $\Phi_a\delta(\boldsymbol{x} - \boldsymbol{x}_a) + \Phi_b\delta(\boldsymbol{x} - \boldsymbol{x}_b)$ and the magnetic field is the superposition of two contributions $\boldsymbol{B}(\boldsymbol{x}) = \boldsymbol{B}_a(\boldsymbol{x}) + \boldsymbol{B}_b(\boldsymbol{x})$. Thus,

$$F_{\text{Charged}} = \int \frac{1}{2}(\boldsymbol{B}_a + \boldsymbol{B}_b)[\Phi_a\delta(\boldsymbol{x} - \boldsymbol{x}_a) + \Phi_b\delta(\boldsymbol{x} - \boldsymbol{x}_b)] = \frac{\Phi_a\Phi_b e^2 w\varrho^2}{2\pi}K_0\left(\frac{|\boldsymbol{x}_2 - \boldsymbol{x}_1|}{\lambda}\right) + E_{va} + E_{vb}, \tag{A15}$$

and $E_{va} \equiv \int \boldsymbol{B}_a(\boldsymbol{x}_a)\Phi_a/2$ denotes the (self-)energy of the vortex a. Finally, the interaction energy of two vortices in components a,b reads as

$$E_{\text{ab}}^{(\text{int}),\text{Charged}} = \frac{2\pi w|\psi_a|^2|\psi_b|^2}{\varrho^2}K_0\left(\frac{|\boldsymbol{x}_a - \boldsymbol{x}_b|}{\lambda}\right). \tag{A16}$$

The interaction of the charged sector is thus a Yukawa-type interaction given by the modified Bessel function. If we do not consider antivortices, it is always positive (for any a,b), then it gives repulsive interaction between any kind of fractional vortices. On the other hand, the interaction through the *neutral* sector is logarithmic. It is attractive (resp. repulsive) for fractional vortices of the different (resp. same) kind. The energy associated with the *neutral* mode (A10b) reads as

$$F_{\text{Neutral}} = \frac{|\psi_1|^2|\psi_2|^2}{2\varrho^2}\int(\nabla\varphi_{12})^2. \tag{A17}$$

A phase winding around some singularity located at the point $\boldsymbol{x}_a$ is (at sufficiently large distance) well approximated by $\varphi_a = \theta$. Thus,

$$\nabla\varphi_a = \frac{\boldsymbol{e}_\theta}{|\boldsymbol{x} - \boldsymbol{x}_a|} = z\times\nabla\ln|\boldsymbol{x} - \boldsymbol{x}_a|. \tag{A18}$$

To evaluate the interaction between fractional vortices in different condensates and respectively located at $\boldsymbol{x}_a$ and $\boldsymbol{x}_b$,

the neutral sector is expanded as

$$F_{\text{Neutral}} = \frac{|\psi_1|^2|\psi_2|^2}{2\varrho^2}\int (\nabla\varphi_a)^2 + (\nabla\varphi_b)^2 - 2\nabla\varphi_a\cdot\nabla\varphi_b. \tag{A19}$$

Thus, the interacting part reads as

$$\begin{aligned} E_{\text{ab}}^{(\text{int}),\text{Neutral}} &= -\frac{|\psi_1|^2|\psi_2|^2}{\varrho^2}\int \nabla\varphi_a\cdot\nabla\varphi_b \\ &= \frac{|\psi_1|^2|\psi_2|^2}{\varrho^2}\int \varphi_a\Delta\varphi_b \\ &= \frac{|\psi_1|^2|\psi_2|^2}{\varrho^2}\int \ln|\boldsymbol{x}-\boldsymbol{x}_a|\delta(|\boldsymbol{x}-\boldsymbol{x}_b|) \\ &= 2\pi\frac{|\psi_1|^2|\psi_2|^2}{\varrho^2}\ln|\boldsymbol{x}_b-\boldsymbol{x}_a|. \end{aligned} \tag{A20}$$

Similarly, the interaction between two vortices in the same condensate a is computed by requiring that the phase is the sum of the individual phases $\varphi_a = \varphi_a^{(1)} + \varphi_a^{(2)}$, while $\varphi_b = 0$. Then, the interaction reads as

$$E_{aa}^{(\text{int}),\text{Neutral}} = -2\pi\frac{|\psi_1|^2|\psi_2|^2}{\varrho^2}\ln\left|\boldsymbol{x}_a^{(2)}-\boldsymbol{x}_a^{(1)}\right|. \tag{A21}$$

To summarize, the interaction of vortices in different condensates is then

$$\frac{E_{12}^{(\text{int})}}{2\pi} = \frac{|\psi_1|^2|\psi_2|^2}{\varrho^2}\left[\ln\frac{r}{R} + wK_0\left(\frac{r}{\lambda}\right)\right], \tag{A22}$$

while interactions of vortices of similar condensates are

$$\frac{E_{aa}^{(\text{int})}}{2\pi} = -\frac{|\psi_1|^2|\psi_2|^2}{\varrho^2}\ln\frac{r}{R} + \frac{w|\psi_a|^4}{\varrho^2}K_0\left(\frac{r}{\lambda}\right), \tag{A23}$$

with $r \equiv |\boldsymbol{x}_a - \boldsymbol{x}_b|$ and R the sample size. Equations (A22) and (A23) give the different interactions between fractional vortices. Finally, choosing the energy scale to be $2\pi|\psi_1|^2|\psi_2|^2/\varrho^2$ and defining the parameters m and w as

$$w = 1 + \nu\varrho^2 = 1 + \nu(|\psi_1|^2 + |\psi_2|^2), \quad m = \frac{|\psi_1|^2}{|\psi_2|^2}. \tag{A24}$$

The interaction between fractional vortices in the various condensates reads as

$$\begin{aligned} E_{11} &= \ln\frac{R}{r} + wmK_0\left(\frac{r}{\lambda}\right), \\ E_{22} &= \ln\frac{R}{r} + \frac{w}{m}K_0\left(\frac{r}{\lambda}\right), \\ E_{12} &= -\ln\frac{R}{r} + wK_0\left(\frac{r}{\lambda}\right). \end{aligned} \tag{A25}$$

Thus, vortex matter in the London limit of a two-component superconductor with intercomponent drag interaction is described by a three-parameter family (m,w,R).

3. Mapping to an easy-plane nonlinear σ model

The bound state of well-separated fractional vortices is a *skyrmion*. This follows from mapping the two-component model (A1a)–(A1d) to an easy-plane nonlinear σ model [11,26]. There, the pseudospin unit vector $\mathbf{n}$ is the projection of superconducting condensates on spin-$\frac{1}{2}$ Pauli matrices $\boldsymbol{\sigma}$:

$$\mathbf{n} \equiv (n_x,n_y,n_z) = \frac{\Psi^\dagger\boldsymbol{\sigma}\Psi}{\Psi^\dagger\Psi}, \quad \text{where} \quad \Psi^\dagger = (\psi_1^*,\psi_2^*). \tag{A26}$$

The following identity is useful to rewrite the free energy (A1a)–(A1d) in terms of the pseudospin $\mathbf{n}$, total density ϱ, and gauge-invariant current $\boldsymbol{J}$:

$$\frac{\varrho^2}{4}\partial_k n_a\partial_k n_a + (\nabla\varrho)^2 = \frac{|\psi_1|^2|\psi_2|^2}{\varrho^2}(\nabla\varphi_{12})^2 + \sum_a(\nabla|\psi_a|)^2, \tag{A27}$$

where summation on repeated indices is implied. Using the definition of the current (A7) and noting that

$$4\varepsilon_{ijk}\partial_i\left(\sum_a\frac{|\psi_a|^2}{\varrho^2}\partial_j\varphi_a\right) = \varepsilon_{ijk}\varepsilon_{abc}n_a\partial_i n_b\partial_j n_c, \tag{A28}$$

where ε is the Levi-Civita symbol, the magnetic field reads as

$$B_k = \frac{1}{e}\varepsilon_{ijk}\left[\partial_i\left(\frac{J_j}{ew\varrho^2}\right) - \frac{1}{4}\varepsilon_{abc}n_a\partial_i n_b\partial_j n_c\right], \tag{A29}$$

and the free energy (A5a)–(A5d) can be written as

$$\begin{aligned} \mathcal{F} = \frac{1}{2}(\nabla\varrho)^2 + \frac{\varrho^2}{8}\partial_k n_a\partial_k n_a + \frac{\boldsymbol{J}^2}{2e^2w\varrho^2} + V(\varrho,n_z) \\ + \frac{1}{2e^2}\left\{\varepsilon_{ijk}\left[\partial_i\left(\frac{J_j}{ew\varrho^2}\right) - \frac{1}{4}\varepsilon_{abc}n_a\partial_i n_b\partial_j n_c\right]\right\}^2, \end{aligned} \tag{A30}$$

where $V(\varrho,n_z)$ stands for the potential terms (A1b) and (A1c). The easy-plane potential explicitly reads as

$$V(\varrho,n_z) = \frac{\varrho^2}{2}(a_1 + a_2n_z) + \frac{\varrho^4}{4}\left(b_1 + 2b_2n_z + b_3n_z^2\right), \tag{A31}$$

with the coefficients

$$\begin{aligned} &b_1 = \frac{\beta_1+\beta_2+\gamma}{2}, \quad b_2 = \frac{\beta_1-\beta_2}{2}, \quad b_3 = \frac{\beta_1+\beta_2-\gamma}{2}, \\ &a_1 = \alpha_1+\alpha_2, \quad a_2 = \alpha_1-\alpha_2. \end{aligned} \tag{A32}$$

The pseudospin configuration defines a map from the one-point compactification of the plane ($\mathbb{R}^2 \simeq S^2$) to the two-sphere target space spanned by $\mathbf{n}$. That is, $\mathbf{n}: S^2 \to S^2$, classified by the homotopy class $\pi_2(S^2) \in \mathbb{Z}$, thus defining the integer-valued topological (skyrmionic) charge

$$\mathcal{Q}(\mathbf{n}) = \frac{1}{4\pi}\int_{\mathbb{R}^2}\mathbf{n}\cdot\partial_x\mathbf{n}\times\partial_y\mathbf{n}\,dx\,dy. \tag{A33}$$

Ordinary (composite) vortices with a single core $\Psi = 0$ have $\mathcal{Q} = 0$. Core split vortices, on the other hand, have nontrivial skyrmionic charge $\mathcal{Q} = N$ (N coincides with the number of carried flux quanta). The calculated pseudospin texture of $\mathbf{n}$ is shown on the rightmost panel in Fig. 6. Numerically calculated topological charge was found to be an integer (with a negligible error of order 10^{-5}). It is worth emphasizing that the topological charge (A33) is an integer, when integrated

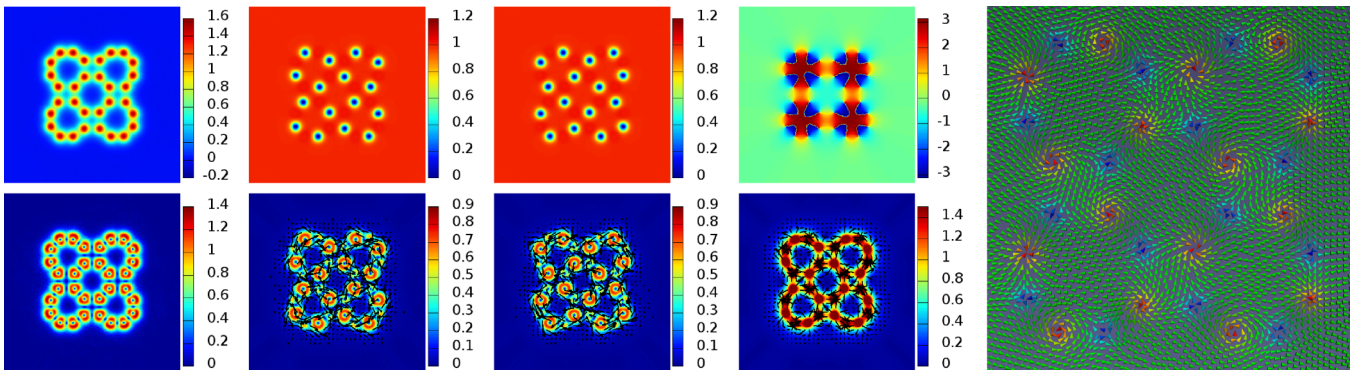

FIG. 6. (Color online) Octagonlike structure carrying $\mathcal{Q} = 16$ flux quanta. The elementary cell here is a $\mathcal{Q} = 4$ skyrmion. The parameters are $(\alpha_a, \beta_a) = (-5.0, 1.0)$ with $e = 0.6$ and Andreev-Bashkin coupling is $\nu = 2.0$, while biquadratic coupling vanish es $\gamma = 0$. Displayed quantities are, respectively, the magnetic field $\boldsymbol{B}$, $|\psi_1|^2$, $|\psi_2|^2$ and the phase difference $\varphi_{12} \equiv \varphi_2 - \varphi_1$, on the first line. On the second line, $\boldsymbol{J}$, $\boldsymbol{J}_1$, $\boldsymbol{J}_2$, and $\mathbf{z} \times \boldsymbol{\nabla}\varphi_{12}$. The rightmost panel shows the normalized projection of $\mathbf{n}$ onto the plane, while colors give the magnitude of n_z. Blue corresponds to the south pole (-1) while red is the north pole $(+1)$ of the target sphere S^2.

over the infinite plane $\mathbb{R}^2$, or at least a large enough domain $\Omega \subset \mathbb{R}^2$. By large enough, we understand that the fields should have recovered their ground-state values at the boundary. Then, the skyrmions shall not interact with the boundary. When the skyrmion's size is comparable with the size of the integration domain, truncation errors appear and $\mathcal{Q}$ is no more an integer. Moreover, when simulating a finite sample in an applied field, in general the skyrmionic topological charge $\mathcal{Q}$ will not be an integer. This is because in general there are states where only a part of the skyrmion texture enters the sample.

APPENDIX B: ADDITIONAL MATERIAL

The biquadratic density interaction (A1c) also induces core splitting of the fractional vortices, for positive couplings γ. Unlike the drag term which induces splitting by energetically penalizing coflowing currents, biquadratic density coupling (with $\gamma > 0$) penalizes core overlap directly. Indeed, it is energetically preferable to have singularities in each component sitting in different positions. Such a term is in general possible in multicomponent systems. Note that when the coupling is strong, it is no more favorable to have coexisting condensates and the superfluid density of a given condensate is completely suppressed (i.e., phase separation).

Unlike the current drag interactions, the physics of the core splitting induced by biquadratic densities can not be captured within the London limit (since it involves only densities). In general, combining both dissipationless drag and biquadratic density interaction widely enriches the spectrum of various skyrmionic structures which can be obtained. Figures 7–12 show detail of multiskyrmion solutions from the main body of the paper.

APPENDIX C: NUMERICAL METHODS

1. Finite-element energy minimization

We consider the two-dimensional problem (A1a)–(A1d) defined on the bounded domain $\Omega \subset \mathbb{R}^2$ with $\partial\Omega$ its boundary. In practice, we choose Ω to be a disk. The problem is

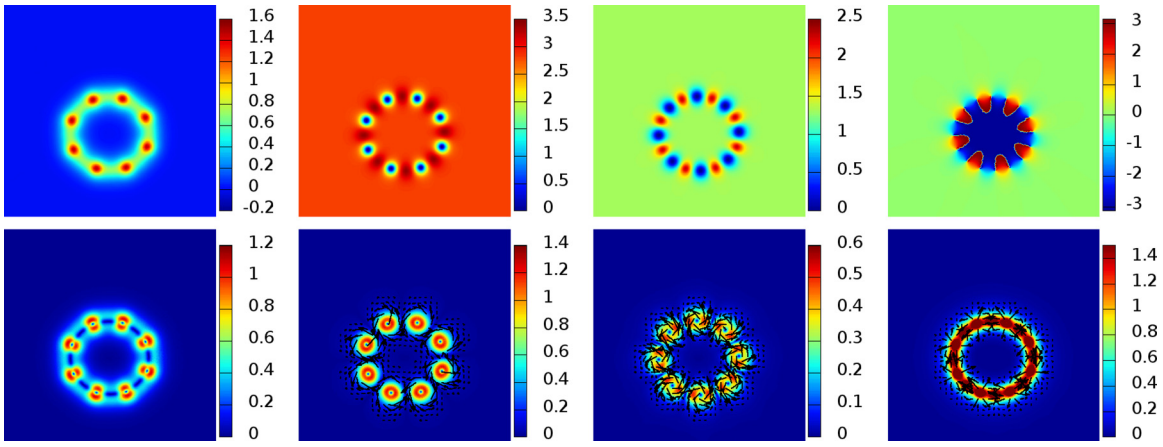

FIG. 7. (Color online) 8-vortex configuration. Parameters are $(\alpha_1, \beta_1) = (-3.6, 1.0)$ and $(\alpha_2, \beta_2) = (-3.0, 1.0)$ and $\gamma = 0.6$ with $e = 0.6$. There is no Andreev-Bashkin coupling $\nu = 0.0$ but fractional vortices are split by biquadratic density coupling only. Displayed quantities are, respectively, the magnetic field $\boldsymbol{B}$, $|\psi_1|^2$, $|\psi_2|^2$, and the phase difference $\varphi_{12} \equiv \varphi_2 - \varphi_1$, on the first line. On the second line, $\boldsymbol{J}$, $\boldsymbol{J}_1$, $\boldsymbol{J}_2$, and $\mathbf{z} \times \boldsymbol{\nabla}\varphi_{12}$.

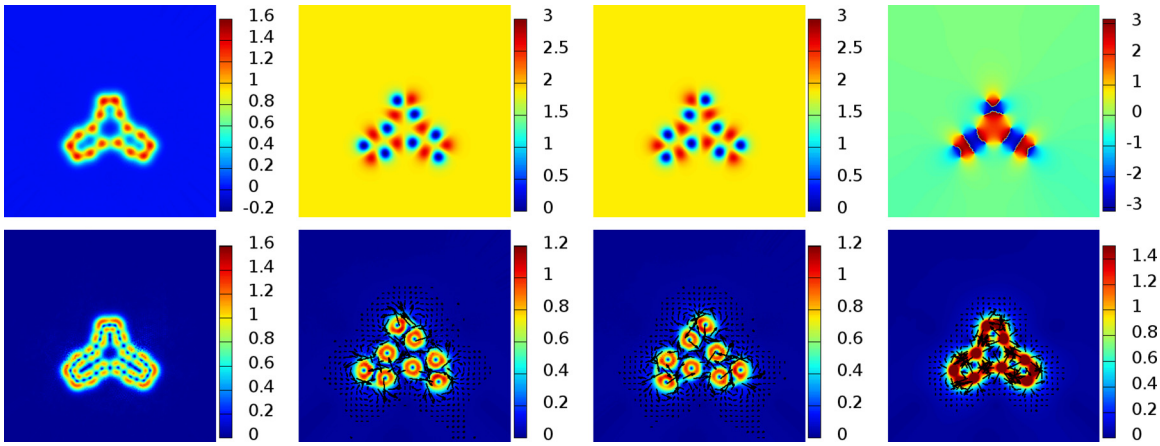

FIG. 8. (Color online) Multiskyrmion carrying $\mathcal{Q} = 8$ flux quanta, for identical components $(\alpha_a, \beta_a) = (-3.0, 1.0)$ and $\gamma = 0.6$ with $e = 0.8$. The Andreev-Bashkin coupling is $\nu = 1.0$. Displayed quantities are the same as in Fig. 7.

supplemented by the boundary condition $\boldsymbol{n} \cdot \boldsymbol{D}\psi_a = 0$ with $\boldsymbol{n}$ the normal vector to $\partial\Omega$. Physically, this condition implies there is no current flowing through the boundary. Since this boundary condition is gauge invariant, an additional constraint can be chosen on the boundary to fix the gauge. Our choice is to impose the radial gauge on the boundary $\boldsymbol{e}_\rho \cdot \boldsymbol{A} = 0$ (note that with our choice of domain, this is equivalent to $\boldsymbol{n} \cdot \boldsymbol{A} = 0$). With this choice, (most of) the gauge degrees of freedom are eliminated and the "no current flow" condition separates in two parts

$$\boldsymbol{n} \cdot \nabla\psi_a = 0 \quad \text{and} \quad \boldsymbol{n} \cdot \boldsymbol{A} = 0. \tag{C1}$$

Note that these boundary conditions allow a topological defect to escape from the domain. To prevent this in simulations of individual skyrmions or skyrmion groups without applied field, the numerical grid is chosen to be large enough so that the attractive interaction with the boundaries is negligible for a given numerical accuracy. Thus, in this method one has to use large numerical grids, which is computationally demanding. The advantage is that it is guaranteed that obtained solutions are not boundary pressure artifacts.

The variational problem is defined for numerical computation using a finite-element formulation provided by the FREEFEM++ library [24]. Discretization within finite-element formulation is done via a (homogeneous) triangulation over Ω, based on Delaunay-Voronoi algorithm. Functions are decomposed on a continuous piecewise quadratic basis on each triangle. The accuracy of such method is controlled through the number of triangles (we typically used $3 \sim 6 \times 10^4$), the order of expansion of the basis on each triangle (second-order polynomial basis on each triangle), and also the order of the quadrature formula for the integral on the triangles.

Once the problem is mathematically well defined, a numerical optimization algorithm is used to solve the variational nonlinear problem (i.e., to find the minima of $\mathcal{F}$). We used here a nonlinear conjugate gradient method. The algorithm is iterated until relative variation of the norm of the gradient of the functional $\mathcal{F}$ with respect to all degrees of freedom is less than 10^{-6}.

Initial guess

The initial field configuration carrying N flux quanta is prepared by using an ansatz which imposes phase windings around spatially separated N vortex cores in each

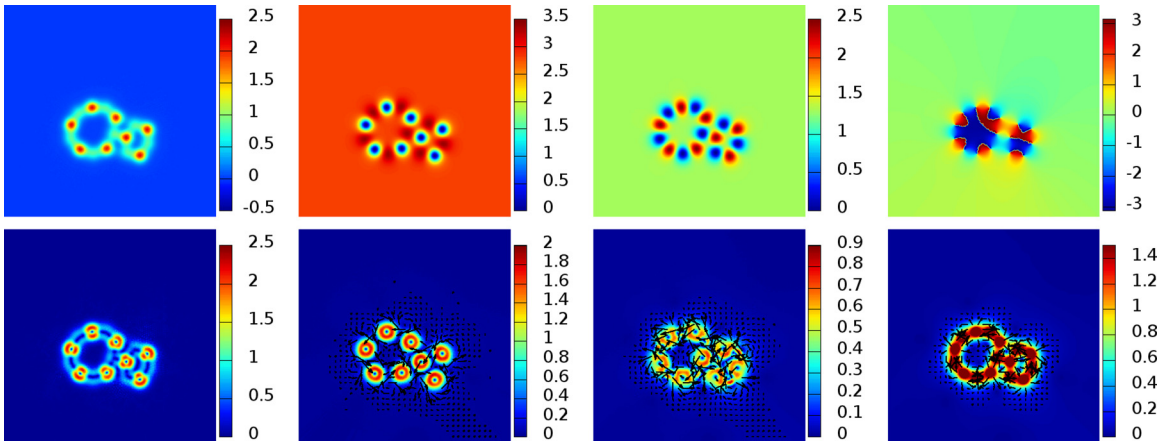

FIG. 9. (Color online) An 8-flux quanta configuration. Displayed quantities and the parameters are the same as in Fig. 7 except for the coupling $\nu = 1$.

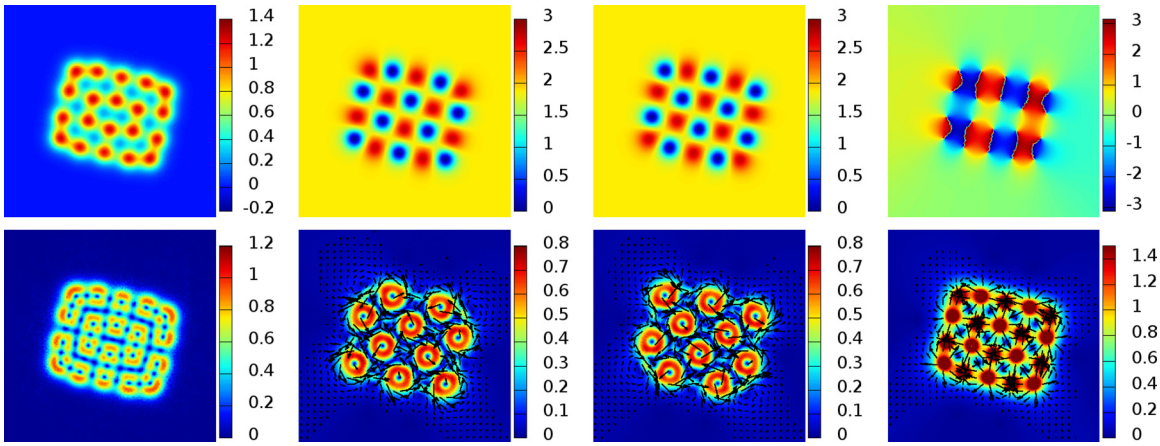

FIG. 10. (Color online) A checkerboard cluster with $\mathcal{Q} = 10$. Parameters are the same as in Fig. 8 except the gauge coupling $e = 0.6$.

condensate:

$$\begin{aligned} \psi_a &= |\psi_a| e^{i\Theta_a}, \\ |\psi_a| &= u_a \prod_{k=1}^{N_v} \sqrt{\frac{1}{2}\left[1 + \tanh\left(\frac{4}{\xi_a}\left[\mathcal{R}_k^a(x,y) - \xi_a\right]\right)\right]}, \end{aligned} \tag{C2}$$

where $a = 1,2$ and u_a is the ground-state value of each condensate density. The parameters ξ_a parametrize the core size while

$$\begin{aligned} \Theta_a(x,y) &= \sum_{k=1}^{N} \tan^{-1}\left(\frac{y - y_k^a}{x - x_k^a}\right), \\ \mathcal{R}_k^a(x,y) &= \sqrt{\left(x - x_k^a\right)^2 + \left(y - y_k^a\right)^2}. \end{aligned} \tag{C3}$$

(x_k^a, y_k^a) determines the position of the core of kth vortex of the a condensate. The starting configuration of the vector potential is determined by solving Ampère's law equation on the background of the superconducting condensates specified by (C2) and (C3). Being a linear equation in $\boldsymbol{A}$, this is an easy operation.

Once the initial configuration is defined, all degrees of freedom are relaxed simultaneously, within the "no current flow" boundary conditions discussed previously, to obtain highly accurate solutions of the Ginzburg-Landau equations.

2. Finite-difference simulations

In our simulations using finite differences, the energy functional (A1a)–(A1d) is discretized in a gauge-invariance preserving manner using forward differences. For details of the discretization scheme, see [52]. The constant applied external magnetic field $\boldsymbol{H} = H\boldsymbol{e}_z$ is fixed by taking advantage of Stokes' theorem and specifying that $\boldsymbol{A}$ on the boundary satisfies

$$\nabla \times \boldsymbol{A} = \boldsymbol{H}. \tag{C4}$$

Stokes' theorem then ensures the flux through the system is equal to $\int_{\Omega \subset \mathbb{R}^2} \boldsymbol{H} \cdot \boldsymbol{dS}$, but allowing $\boldsymbol{A}$ and hence $\boldsymbol{B}$ to vary arbitrarily inside the system. Note that this leaves gauge degrees of freedom in the system. However, in an energy minimization problem, the algorithm only considers the energy which is a gauge-invariant quantity. Thus, the possibility

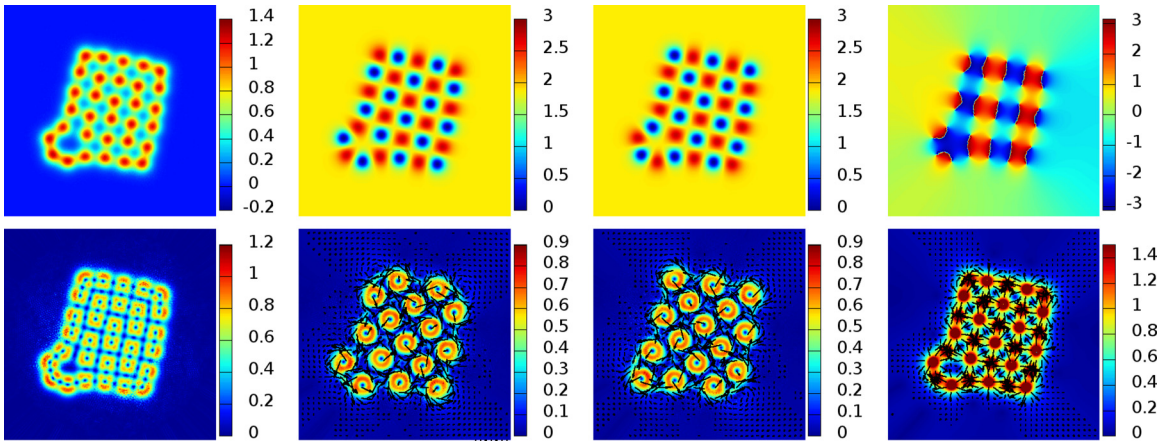

FIG. 11. (Color online) $\mathcal{Q} = 16$ skyrmions. The system compromises between the optimal compact packing and the number of vortices by creating a small loop at one of the corners. Parameters are the same as in Fig. 10.

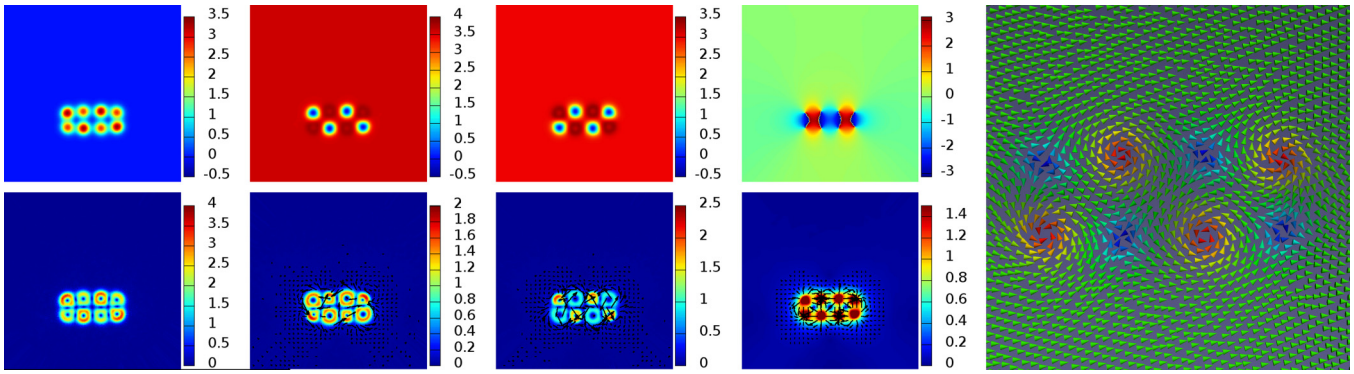

FIG. 12. (Color online) A 4-quanta $\mathcal{Q} = 4$ configuration. Parameters are $(\alpha_1,\beta_1) = (-3.6,1.0)$, $(\alpha_2,\beta_2) = (-3.0,1.0)$ with $e = 0.3$, and Andreev-Bashkin coupling is $\nu = 5.0$. Biquadratic coupling vanishes $\gamma = 0$. Displayed quantities are the same as in Fig. 6.

of evolving simply by a gauge transformation is eliminated since it does not lower the energy. The boundary condition is the discrete equivalent of $\boldsymbol{n} \cdot \boldsymbol{D}\psi_a = 0$ and ensures that no supercurrent escapes the sample. This boundary is located several lattice points inside the computational lattice. This is the boundary of the sample and outside it, ψ_i are not solved for.

The lattice parameters h_i control the accuracy of the lattice approximation, and the minimization algorithm is considered to be converged whenever the largest discrete gradient in the system is below $10^{-5}\Pi_i h_i$ or the sup-norm of the discrete gradients is below 10^{-7}. Some control calculations with a more restrictive convergence criterion were made but with no appreciable change to the solutions.

We typically used domains of 401×403 lattices points with lattice spacing of $h_i = 0.1$. As an initial configuration, we set $\psi_a = 0$ outside the superconductor (these values are not part of the minimization process), $\boldsymbol{A} = 0$ everywhere, and $\psi_a = \sqrt{\frac{\alpha_a}{\beta_a}} \exp i\varphi_a(x,y)$, where phases $\varphi_a(x,y) \in [-\pi,\pi)$ are randomly chosen. At the beginning, therefore, we have $\boldsymbol{B} = 0$ and this corresponds to a zero-field-cooled sample. When we have found a solution at a given external field, the boundary condition for $\boldsymbol{A}$ is updated to reflect the new field and the old solution is used as an initial guess for the next solution. A quasi-Newton algorithm with BFGS Hessian updates is used to simultaneously solve for all degrees of freedom subject to the boundary conditions at the two different boundaries (one for $\boldsymbol{A}$ and one for Ψ). The program itself is an extension of the one used in [42] (for further details, see [42] and the relevant references therein).

3. Monte Carlo simulations

In the Monte Carlo simulations, vortices are treated as a system of N point particles of two different colors, interacting with potentials (A25). The point particles live in a two-dimensional box $L \times L$ so that the number of particles per surface area is N/L^2. Periodic boundary conditions are imposed and the interaction is cut at half the box width. Tests with open boundary conditions without a cutoff have been performed and no structural differences are noted as compared to low-density simulations with periodic boundary conditions. Data are acquired during at least 10^4 sweeps (a sweep constitutes a number of trial moves equal to the number of particles in the box), after an equilibration from a random initial configuration. The Monte Carlo trial moves consist of a single-particle displacement, a pairwise displacement of a nearest-neighbors bound pair, or rotation of such a pair. The number of particles remains unchanged during the simulation. Furthermore, the maximal step length of a displacement is controlled such that approximately 10% of the displacement trial moves are accepted. Parallel tempering is used in order for the low-temperature simulations to quickly converge into ordered low-energy states, as a low-temperature simulation of these systems can easily be trapped in a metastable state.

The square lattice order parameter is defined as

$$\Psi_4 = \frac{1}{4N}\left|\sum_{i=1}^{N}\sum_{j=1}^{4}\exp(4i\phi_{ij})\right|, \tag{C5}$$

where the sum in j runs over the four nearest neighbors of particle i, and ϕ_{ij} is the angle of the line joining particles i,j with some arbitrary axis.

[1] A. F. Andreev and E. P. Bashkin, JETP **42**, 164 (1975).
[2] A. J. Leggett, Ann. Phys. (NY) **46**, 76 (1968).
[3] A. J. Leggett, Rev. Mod. Phys. **47**, 331 (1975).
[4] S. B. Chung, H. Bluhm, and E.-A. Kim, Phys. Rev. Lett. **99**, 197002 (2007).
[5] S. B. Chung, D. F. Agterberg, and E.-A. Kim, New J. Phys. **11**, 085004 (2009).
[6] O. Sjöberg, Nucl. Phys. A **265**, 511 (1976).
[7] N. Chamel, Mon. Not. R. Astron. Soc. **388**, 737 (2008).
[8] M. A. Alpar, S. A. Langer, and J. A. Sauls, Astrophys. J. **282**, 533 (1984).
[9] M. G. Alford and G. Good, Phys. Rev. B **78**, 024510 (2008).
[10] E. Babaev, Phys. Rev. D **70**, 043001 (2004).
[11] E. Babaev, Phys. Rev. B **79**, 104506 (2009).
[12] E. V. Herland, E. Babaev, and A. Sudbø, Phys. Rev. B **82**, 134511 (2010).

[13] D. V. Fil and S. I. Shevchenko, Phys. Rev. A **72**, 013616 (2005).
[14] P. P. Hofer, C. Bruder, and V. M. Stojanović, Phys. Rev. A **86**, 033627 (2012).
[15] A. B. Kuklov and B. V. Svistunov, Phys. Rev. Lett. **90**, 100401 (2003).
[16] A. Kuklov, N. Prokof'ev, and B. Svistunov, Phys. Rev. Lett. **93**, 230402 (2004).
[17] A. Kuklov, N. Prokof'ev, and B. Svistunov, Phys. Rev. Lett. **92**, 030403 (2004).
[18] E. K. Dahl, E. Babaev, and A. Sudbø, Phys. Rev. Lett. **101**, 255301 (2008).
[19] E. K. Dahl, E. Babaev, and A. Sudbø, Phys. Rev. B **78**, 144510 (2008).
[20] E. K. Dahl, E. Babaev, S. Kragset, and A. Sudbo, Phys. Rev. B **77**, 144519 (2008).
[21] A. B. Kuklov, N. V. Prokof'Ev, B. V. Svistunov, and M. Troyer, Ann. Phys. (NY) **321**, 1602 (2006).
[22] E. Babaev, Phys. Rev. Lett. **89**, 067001 (2002).
[23] E. Babaev, Nucl. Phys. B **686**, 397 (2004).
[24] F. Hecht, J. Numer. Math. **20**, 251 (2012).
[25] E. Babaev, J. Jäykkä, and M. Speight, Phys. Rev. Lett. **103**, 237002 (2009).
[26] E. Babaev, L. D. Faddeev, and A. J. Niemi, Phys. Rev. B **65**, 100512 (2002).
[27] A. Knigavko and B. Rosenstein, Phys. Rev. Lett. **82**, 1261 (1999).
[28] Q. Li, J. Toner, and D. Belitz, Phys. Rev. Lett. **98**, 187002 (2007).
[29] A. Knigavko, B. Rosenstein, and Y. F. Chen, Phys. Rev. B **60**, 550 (1999).
[30] Q. Li, J. Toner, and D. Belitz, Phys. Rev. B **79**, 014517 (2009).
[31] B. Rosenstein, I. Shapiro, B. Ya. Shapiro, and G. Bel, Phys. Rev. B **67**, 224507 (2003).
[32] J. Garaud and E. Babaev, Phys. Rev. B **86**, 060514 (2012).
[33] J. Garaud, J. Carlström, E. Babaev, and M. Speight, Phys. Rev. B **87**, 014507 (2013); Phys. Rev. Lett. **107**, 197001 (2011).
[34] M. Kobayashi and M. Nitta, Phys. Rev. D **87**, 085003 (2013).
[35] T. A. Tokuyasu, D. W. Hess, and J. A. Sauls, Phys. Rev. B **41**, 8891 (1990).
[36] J. Carlström, J. Garaud, and E. Babaev, Phys. Rev. B **84**, 134515 (2011).
[37] J. Carlström, J. Garaud, and E. Babaev, Phys. Rev. B **84**, 134518 (2011).
[38] J. Garaud, D. F. Agterberg, and E. Babaev, Phys. Rev. B **86**, 060513 (2012).
[39] D. F. Agterberg, Phys. Rev. B **58**, 14484 (1998).
[40] J. Jäykkä and M. Speight, Phys. Rev. D **82**, 125030 (2010).
[41] D. J. Earl and M. W. Deem, Phys. Chem. Chem. Phys. **7**, 3910 (2005).
[42] H. Palonen, J. Jäykkä, and P. Paturi, Phys. Rev. B **85**, 024510 (2012).
[43] M. Ichioka, Y. Matsunaga, and K. Machida, Phys. Rev. B **71**, 172510 (2005).
[44] S. B. Chung and S. A. Kivelson, Phys. Rev. B **82**, 214512 (2010).
[45] M. A. Silaev, Phys. Rev. B **83**, 144519 (2011).
[46] See Supplemental Material at http://link.aps.org/supplemental/10.1103/PhysRevB.89.104508 for animations of the magnetization process.
[47] V. O. Dolocan, C. Veauvy, F. Servant, P. Lejay, K. Hasselbach, Y. Liu, and D. Mailly, Phys. Rev. Lett. **95**, 097004 (2005).
[48] P. G. Björnsson, Y. Maeno, M. E. Huber, and K. A. Moler, Phys. Rev. B **72**, 012504 (2005).
[49] C. W. Hicks, J. R. Kirtley, T. M. Lippman, N. C. Koshnick, M. E. Huber, Y. Maeno, W. M. Yuhasz, M. B. Maple, and K. A. Moler, Phys. Rev. B **81**, 214501 (2010).
[50] P. J. Curran, V. V. Khotkevych, S. J. Bending, A. S. Gibbs, S. L. Lee, and A. P. Mackenzie, Phys. Rev. B **84**, 104507 (2011).
[51] S. Ray, A. Gibbs, S. Bending, P. Curran, E. Babaev, C. Baines, A. Mackenzie, and S. Lee [Phys. Rev. B (to be published)].
[52] J. Jäykkä, J. Hietarinta, and P. Salo, Phys. Rev. B **77**, 094509 (2008).